Published in final edited form as:
Ann Neurol. 2011 November ; 70(5): 764–773. doi:10.1002/ana.22521.

Multiple Sclerosis Normal-Appearing White Matter: Pathology-Imaging Correlations

Natalia M. Moll, MD, PhD[1,*], **Anna M. Rietsch, BS**[1], **Smitha Thomas, MD**[2], **Amy J. Ransohoff**[1], **Jar-Chi Lee, MS**[3], **Robert Fox, MD**[4], **Ansi Chang, MD**[5], **Richard M. Ransohoff, MD**[1,4], and **Elizabeth Fisher, PhD**[2]

[1]Neuroinflammation Research Center and Department of Neurosciences, Lerner Research Institute, Cleveland Clinic, Cleveland, OH, USA

[2]Department of Biomedical Engineering, Lerner Research Institute, Cleveland Clinic, Cleveland, OH, USA

[3]Department of Quantitative Health Sciences, Lerner Research Institute, Cleveland Clinic, Cleveland, OH, USA

[4]Mellen Center for Multiple Sclerosis Treatment and Research, Neurological Institute, Cleveland Clinic, Cleveland, OH, USA

[5]Department of Neurosciences, Lerner Research Institute, Cleveland Clinic, Cleveland, OH, USA

Abstract

Objective—To determine the pathologic basis of subtle abnormalities in magnetization transfer ratio (MTR) and diffusion tensor imaging (DTI) parameters observed in normal-appearing white matter (NAWM) in multiple sclerosis (MS) brains.

Methods—Brain tissues were obtained through a rapid post-mortem protocol that included *in situ* MRI. Four types of MRI-defined regions of interest (ROIs) were analyzed: (1) Regions that were abnormal on all images ("T2T1MTR lesions"); (2) NAWM regions with slightly-abnormal MTR located close to white matter lesions ("sa-WM Close"); (3) NAWM regions with slightly-abnormal MTR located far from lesions ("sa-WM Far"); and (4) NAWM regions with normal MTR ("NAWM").

Immunohistochemical analysis for each ROI comprised immunostaining for myelin, axonal markers, activated microglia/macrophages, astrocytes, plasma proteins and blood vessels.

Results—Forty-eight ROIs from four secondary progressive MS brains were analyzed. Sa-WM Close ROIs were associated with significantly more axonal swellings. There were more enlarged MHCII(+) microglia and macrophages detected in sa-WM Far, sa-WM Close, and T2T1MTR lesions than in NAWM. Across all ROIs, MTR and DTI measures were moderately correlated with myelin density, axonal area and axonal counts. Excluding T2T1MTR lesions from analysis revealed that MTR and DTI measures in non-lesional WM were correlated with activated microglia, but not with axonal or myelin integrity.

Interpretation—The pathologic substrates for MRI abnormalities in NAWM vary based on distance from focal WM lesions. Close to WM lesions, axonal pathology and microglial activation

CORRESPONDING AUTHOR Elizabeth Fisher, PhD Department of Biomedical Engineering, ND20 Cleveland Clinic Lerner Research Institute 9500 Euclid Avenue Cleveland, OH 44195 USA Telephone: (216) 445-3217 Fax: (216) 445-3224 fishere@ccf.org .
[*]Present address: CRICM / INSERM-UPMC, UMRS 975, Faculté de Médecine Pierre et Marie Curie, Hôpital Pitié-Salipêtrière, Paris, France

may explain subtle MRI changes. Distant from lesions, microglial activation associated with proximity to cortical lesions might underlie MRI abnormalities.

INTRODUCTION

Multiple sclerosis (MS) is the major cause of non-traumatic neurological disability in young adults in Europe and North America.(1;2) Pathologically, MS is characterized by focal white matter (WM) plaques along with diffuse WM injury and cortical demyelination.(3;4) Despite retaining myelin, regions of macroscopically normal-appearing WM (NAWM) in MS often exhibit chronic injury, characterized by the presence of axonal spheroids and swellings, mild inflammation, microglial activation, gliosis and increased expression of proteolytic enzymes.(5) NAWM injury in MS patients is associated with an intrathecal inflammatory reaction that occurs typically behind a grossly intact BBB, as judged by the low incidence of gadolinium-enhancing lesions in late-stage MS. This type of injury is considered to be resistant to currently-available anti-inflammatory and immunomodulatory treatment(6;7) and has been linked to axonal transection within WM lesions leading to secondary Wallerian-like degeneration.(8-10)

Focal WM lesions are readily apparent on conventional magnetic resonance images (MRI) of the brain in MS.(11-14) However, there are only modest correlations between MRI-visible lesions and neurologic deficit, partly due to undetected tissue damage in the NAWM. Non-conventional MRI approaches such as magnetization transfer ratio (MTR) and diffusion tensor imaging (DTI) allow for examination of NAWM *in vivo*.(15-17) MRI changes in MS NAWM include reduced MTR, changes in the diffusion properties of water, alterations in T1 and T2 relaxation times, and reduced *N*-acetyl aspartate.(18-22) MRI abnormalities in normal-appearing brain tissue are clinically relevant. MTR histogram analysis consistently reveals significant differences in MS patients compared to healthy controls which worsen over the course of disease.(6;23) The MTR peak position is shifted slightly lower (90-95% of MTR peak position in controls) and the relative peak height is reduced. Studies of MS patients have shown that WM and gray matter (GM) MTR abnormalities are associated with disability(24) and GM MTR is an independent predictor of disability progression over 8 years.(25)

MTR is heterogeneously reduced in both MS lesions and NAWM. Focally demyelinated MS plaques have severely reduced MTR (20-80% of NAWM MTR). Early animal studies and MRI-pathology correlation studies of MS lesions reveal strong correlations between MTR and myelin content.(26-29) For reasons that remain uncertain, some MTR reductions precede lesion formation.(30) NAWM MTR changes vary with distance from lesions, such that NAWM around MR-defined lesions has significantly lower MTR than NAWM distant from lesions.(31) However, the pathologic substrate of subtle MRI abnormalities in MS NAWM, such as the overall downward shift in MTR histogram peak by 5-10%, has not yet been identified.

In our previous studies on MRI-pathology correlations, we focused on MR-visible lesions.(32-34) Our current research aims to determine the pathologic correlates of MRI abnormalities in NAWM through examination of autopsy brain tissue from patients with SPMS. Brain tissue for this study was imaged and processed according to the protocol we used in our previous studies using image-guided tissue sampling.(32-34) Therefore, rather than the classic histopathologic definition of NAWM, we used standard radiologic criteria to define NAWM as regions that appear normal on T2-weighted MRI. In this study we specifically analyzed WM that is normal on T2-weighted images but slightly abnormal on MTR, including regions both close to and far from lesions, and compared these to regions at extremes of tissue injury, classified as focal MRI-visible lesions or NAWM with normal

MTR. In addition to MTR, DTI measures were investigated to provide further insights into the pathologic correlates of MRI abnormalities commonly detected in NAWM.

MATERIALS AND METHODS

Tissue and tissue acquisition

Collection and use of human tissue was approved by Cleveland Clinic Institutional Review Board. We applied the same tissue acquisition protocol as described previously.(32) In brief, consent was obtained from each tissue donor prior to death or from the next-of-kin. Following notice of tissue donor death, the body was transported to Cleveland Clinic imaging facility where *in situ* MRI of the brain was performed. The cadaver was then delivered for rapid autopsy. The brain and spinal cord were removed and immediately fixed in 4% paraformaldehyde for at least eight weeks. A second MRI of the brain was acquired post-fixation in a custom-designed slicing box just before the brain was cut into 10mm thick coronal sections. Each slice was numbered, stored and subsequently photographed. The cadaver images were registered to the post-fixation images and reformatted to obtain image planes that corresponded with each tissue slice, as previously described.(32) MRI-based region maps were generated to indicate ROIs for immunohistochemical analysis.

MRI: acquisition and analysis

Imaging was performed just prior to autopsy on a 1.5T scanner (Siemens, Erlangen, Germany). The protocol consisted of 3D T1-weighted MPRAGE, T2-weighted 2D FLAIR, an MTR image calculated from PD-weighted 3D gradient echo images acquired with and without an MT pulse *(*7.68ms 250Hz Gaussian applied 1.5kHz off resonance; H1=8.8μT*)*, and a standard 6-direction DTI study, with echo planar images acquired 8 times each and averaged to improve signal-to-noise (maximum b-value = 1000 s/mm^2). The resolution of the MPRAGE image was 1mm^3, FLAIR and MTR were 0.9mm × 0.9mm × 3mm, and DTI was 1.9mm × 1.9mm × 3mm. The DTI dataset was used to calculate fractional anisotropy (FA), mean diffusivity (MD), axial diffusivity ($\lambda\parallel$), and radial diffusivity ($\lambda\perp$) images.

Image characteristics were used to generate region maps to guide tissue sampling. First, the brain was segmented in the FLAIR image(35) and then further segmented into WM lesions and normal-appearing brain tissue. To normalize the MTR values across patients, MTR contrast ratio (CR) images were generated by substituting each voxel intensity with the ratio of the voxel MTR to the mean MTR in NAWM. The FLAIR-identified WM lesions were superimposed on the T1-weighted and MTR images and each lesion was analyzed to identify voxels within the lesion mask that had intensities at least one standard deviation lower than the surrounding NAWM. Lesions which were abnormal on FLAIR, T1 and MTR images were classified as T2T1MTR regions. The lesion mask was also used to create a 3D Euclidean distance map (EDM) which provided the distance of each NAWM voxel from the nearest WM lesion edge. Cortical GM lesions were not considered in the MRI analysis or distance maps because cortical lesions could not be detected using the imaging sequences applied in this study.

ROIs selected for immunohistochemical analysis were manually traced using information from combined lesion and NAWM masks and from the EDM and MTR CR images. A new class of “slightly abnormal” NAWM voxels was defined based on MTR CR in order to identify voxels contributing to the slight downward shift in the MTR histogram, as illustrated in Figure 1. Four types of MRI-based ROIs were defined for comparison: (1) **NAWM:** regions consisting of NAWM voxels with normal MTR (MTR CR ≥ 98%) and located far from visible WM lesions; (2) **sa-WM Far:** regions consisting of NAWM voxels with slightly-abnormal MTR (MTR CR between 90 and 97%) and located far from visible

WM lesions (distance ≥ 5mm); (3) **sa-WM Close:** regions consisting of NAWM voxels with slightly-abnormal MTR (MTR CR between 90 and 97%) and located in close proximity to WM lesions (distance between 1-4mm); and (4) **T2T1MTR:** regions consisting of lesion voxels that were abnormal on T2, T1, and MTR images, as described above.

Forty-eight ROIs were selected and isolated from postmortem MRIs of four MS brains. For each brain, three tissue slices were examined. Four ROIs (one of each type) were sampled from each slice. Thus, in total, there were 12 ROIs analyzed for each brain.

Immunohistochemistry

Using the MRI-based region maps as a guide, ROIs were identified and isolated from the MS brains. Tissue blocks were cryoprotected overnight in 20% glycerol, embedded in 30% sucrose, and sectioned 30μm thick. These sections were used for immunoperoxidase histochemistry and immunofluorescence.

Sections were pretreated as described previously,(36) incubated with primary antibodies for 5 days at 4°C, then incubated with biotinylated secondary antibodies and immunostained by avidin-biotin complex (Vector Laboratories, Burlingame, CA). Diaminobenzidine (Sigma-Aldrich, St Louis, MO) was used as chromogen. Sections for confocal analysis were pretreated as described earlier (hydrogen peroxide was amended), immunostained for 3 days at 4°C, then incubated with secondary antibody conjugated to Alexa Fluor® 594 (Invitrogen, Carlsbad, CA). Primary antibodies used for immunostaining are summarized in Table 1.

Quantitative analysis

Multiple micrographs of each ROI immunostained with neurofilament-H antibodies were imaged using 100x objective and 2.5zoom on Leica SP5 confocal microscope (Germany). Single optical slices of the ROIs were used for quantitative analysis of neurofilaments. Micrographs of ROIs stained with anti-MBP and anti-MHCII antibodies were digitized using 20x objective (Leica DM 4000B, Germany). Microphotographs were taken from four (Neurofilaments) to five (MBP, MHCII) non-overlapping microscopical fields of each ROI. ROIs immunostained against GLUT-1 were scanned using 10x objective on Leica DM5500B with motorized x,y stage, operated through Image-Pro Plus. One mosaic image (average of 150 single images) was acquired for each ROI.

The micrographs were transferred to workstation and quantified using count/measure features of ImagePro Plus (MediaCybernmetics). Initially, area ranges for each antibody were chosen empirically to ensure that the automatically determined Image-Pro counted cell / neurofilament / vessel number correlated with the manual count. Immunopositive structures within the gated area ranges were outlined and assessed by an investigator. MHCII-positive cells more than 5000 pixels^2 in size corresponded to activated microglia and macrophages. Neurofilament-H-positive axons which occupied areas more than 2000 pixels^2 were considered to be swollen, pathologically enlarged axons. Automated quantification of swollen axons in Image Pro was followed by manual correction because axons of normal diameter but oriented longitudinal to the imaging plane would otherwise be counted as enlarged. Therefore, in sections with a mixture of axially and longitudinally oriented axons, longitudinally oriented axons with normal diameter were eliminated from the enlarged axon count. Elements intersected by the upper and/or left edge were not measured. Total area of immunopositive elements was calculated for each ROI and each antibody, as was a sum total of all selected areas in μm^2. Mean area was determined for each ROI and each antibody by dividing the total area by the number of axons or cells. Quantitative analysis of MPB immunoreactivity was performed by automated measurement

of pixel density, which was expressed as the percentage of MBP immunopositive area to the total area.

Statistical analysis

We applied a negative binomial regression using the SAS® procedure GENMOD to determine differences in axonal counts in the studied MS ROIs. Percent of pathologically swollen axons were compared in the ROIs using repeated measures mixed model. Partial Spearman's correlation coefficients (r) were calculated to determine correlations between MRI measurements and pathology with adjustment for correlated samples. The proportion of enlarged activated microglial cells were compared across ROI region types using logistic regression analysis. $p<0.05$ was considered statistically significant

RESULTS

MRI-pathology correlations were performed on brain tissue acquired from four patients with secondary progressive MS (two males and two females; mean age 52.5±9.8 years; MS duration 27.2±14.2 years). The demographic and clinical details on these patients are provided in Table 2. The mean postmortem time to fixation was 5.8±1.0 hours, including MRI. The 48 selected ROIs had the following characteristics: **NAWM:** n=12, mean MTR CR = 1.0±0.03, mean distance from closest lesion voxels = 10.1±3.7mm; **sa-WM Far**: n=12, mean MTR CR = 0.95±0.04, mean distance from closest lesion voxels = 5.8±3.2mm; **sa-WM Close**: n=12, mean MTR CR = 0.95±0.03; mean distance from closest lesion voxels = 2.9±1.5mm; **T2T1MTR:** n=12, mean MTR CR = 0.65±0.1; mean distance from closest lesion voxels = 0.2±0.2mm. Representative ROIs for each type and their corresponding histopathologic features are shown in Figure 2.

In sa-WM Close, abnormal MTR is associated with axonal pathology

T2T1MTR regions were associated with an increased number of pathologically swollen axons (larger than 2000 pixels^2) as compared with NAWM ($p<0.001$) and sa-WM Far regions ($p<0.01$). sa-WM Close regions also contained significantly more pathologically swollen axons as compared with sa-WM Far ($p=0.02$) and NAWM ($p=0.004$) (Figure 3). sa-WM Close and T2T1MTR regions were not significantly different in terms of the numbers of swollen axons. When looking at the overall axonal counts, T2T1MTR lesions had significantly fewer axons as compared with other ROIs (Figure 4) and there was a trend for sa-WM Close regions to have fewer axons compared to NAWM regions. MTR and all four DTI measures correlated with axon density, with correlation coefficients ranging from $r=0.42$ ($p=0.003$) for $\lambda\parallel$ to $r=0.58$ ($p<0.0001$) for MTR. (Table 3)

MTR and DTI measures were also moderately correlated with mean axonal area. Larger axonal diameter was associated with lower MTR ($r=-0.46$, $p=0.001$) higher MD ($r=0.47$, $p < 0.001$) and lower FA ($r=-0.41$, $p=0.004$). Radial and axial diffusivities ($\lambda\perp$ and $\lambda\parallel$), from which FA and MD were derived, were both positively correlated with mean axonal area ($r=0.46$, $p=0.001$ for $\lambda\perp$; $r=0.38$, $p=0.008$ for $\lambda\parallel$) However, when the T2T1MTR regions were excluded from analysis and only sa-WM and NAWM, i.e. non-lesional, ROIs were considered, correlations between mean axonal area and MRI measures were no longer significant.

sa-WM Far and sa-WM Close ROIs correspond to regions with increased numbers of activated microglia

The total number of MHCII(+) microglia and macrophages did not differ significantly between different types of ROIs (Supplementary Figure 1). However, sa-WM Far, sa-WM

Close, and T2T1MTR regions contained significantly higher numbers of enlarged activated microglial cells (> 5000 pixels^2) as compared with NAWM ($p<0.05$;Table 4).

Mean MHCII area was not correlated with any of the DTI and MTR measures when all ROIs were considered. However, when T2T2MTR ROIs were excluded and only sa-WM and NAWM regions were considered in the analysis, mean MHCII area was correlated with FA and axial diffusivity, $\lambda\|$ ($r=-0.33$, $p=0.05$ for FA; $r=-0.38$, $p=0.03$ for $\lambda\|$; Figure 5).

Myelin status of slightly abnormal NAWM in MS brains

In NAWM ROIs, 81.5±1.7% of region area was occupied by MBP immunoreactivity (Figure 2, panel D1). sa-WM Close and sa-WM Far corresponded to areas of macro- and microscopically normal myelin, with 82.5±2.0% and 84.1±1.1% of region area occupied by MBP, respectively (Figure 2, panels B1 and C1). In contrast, all T2T1MTR ROIs corresponded to demyelinated lesions (Figure 2, panel A1). The area occupied by MBP-immunostaining in T2T1MTR ROIs was 6.8±1.4%, which was significantly lower than other types of ROIs ($p<0.0001$).

MTR, FA and MD were correlated with MBP density ($r=0.49$, $p= 0.01$ for MTR; $r=0.38$, $p=0.009$ for FA; $r=-0.41$, $p=0.005$ for MD). Higher radial and axial diffusivities were associated with lower MBP density ($r=-0.51$, $p<0.001$ for radial diffusivity and $r=-0.34$, $p=0.02$ for axial diffusivity). When only sa-WM and NAWM regions were considered in the analysis and the twelve T2T1MTR regions were excluded, there were no correlations between MBP density and MRI measures.

Sa-WM Close and Far neighbor demyelinated cortical lesions

All sa-WM Far as well as many sa-WM Close ROIs were located in close proximity to the cortex. We found that seven sa-WM Far and three sa-WM Close ROIs were adjacent to demyelinated cortical lesions (leucocortical, intracortical or subpial lesions) (Supplementary Figure 2). Two sa-WM Far regions were located near focal areas of MHCII(+) cell activation and expansion and reduced MBP-immunoreactivity on subsequent sections.

Astrogliosis and vascular changes in T2T1MTR and sa-WM

Most T2T1MTR ROIs were associated with reactive astrocytes and gliosis. On the other hand, only individual scattered reactive astrocytes were found in sa-WM Close and sa-WM Far ROIs.

GLUT-1(+) blood vessel number and size were not significantly different in studied ROIs. In T2T1MTR ROIs, there were 40.1±2.9 vessels/mm^2 compared to 46.4±5.8 vessels/mm^2 in NAWM (n.s.). Similarly, vessel sizes ranged from 989±72.5 um^2 in T2T1MTR lesions to 1171.4±157.9 um^2 in NAWM (Supplementary Table 1). Plasma protein immunostaining revealed “leaky” vessels in all studied ROIs, including NAWM regions. Patterns of the plasma protein distribution were different in T2T1MTR and other ROIs: diffuse in T2T1MTR but vasculocentric and focal in sa-WM Close, sa-WM Far and NAWM (Supplementary Figure 3).

DISCUSSION

The pathologic substrates of *subtle* MTR and DTI abnormalities in NAWM of MS brains have not been specifically addressed in previous MRI-pathology correlation reports. The present study used image-guided sampling of MS brain tissue acquired through rapid autopsy to investigate the pathologic correlates of these MRI characteristics in non-lesional WM. The following observations were made: (i) the pathologic substrates for subtle MTR

abnormality in MS NAWM vary depending on proximity to WM lesions; (ii) reduced MTR is associated with axonal swelling in NAWM regions close to WM lesions but not in regions far from WM lesions; (iii) NAWM regions with reduced MTR (either far from or close to lesions) have increased numbers of enlarged microglia / macrophages, and the density of enlarged microglia correlates with DTI measures; (iv) regions of NAWM with reduced MTR often neighbor demyelinating cortical lesions. These findings suggest that a portion of the MTR abnormality in MS NAWM can be accounted for by axonal degeneration and microglial activation. Chronic cortical plaques might also contribute indirectly to reducing MTR in subcortical NAWM by activating nearby microglia. We did not observe significant differences in myelin density, blood vessel number, or plasma IgG deposition ("leaky" vessels) in NAWM regions with slightly abnormal MTR as compared to NAWM regions with normal MTR. Numbers of astrocytic glial cells did not differ in the studied NAWM ROIs.

Consistent with prior reports,(32) we confirmed that there are fewer axons in T2T1MTR lesions as compared to NAWM. We did not find significant differences in axonal counts between the three types of non-lesional WM ROIs (sa-WM Close, sa-WM Far and NAWM ROIs). However, there were more swollen axons in both T2T1MTR lesions and sa-WM Close ROIs as compared with sa-WM Far and NAWM ROIs (Figure 3). In earlier morphological studies of MS brains and spinal cord, reduced axonal density and swollen degenerating axons were found around demyelinated plaques and within defined fiber tracts emerging from plaques.(2;3)(9)(37) Our current observations are generally in line with previous reports and suggest that MTR abnormality in NAWM around MS lesions might partly be explained by axonal destruction in the lesions followed by secondary axonal degeneration and increase in axonal water in peri-plaque WM.

In the present study of MRI correlates of pathology, we did not find differences in myelin, astrogliosis or vascular changes in sa-WM Close or sa-WM Far ROIs as compared with NAWM ROIs. On the other hand, sa-WM ROIs were associated with microglial activation, as indicated by significantly increased density of activated MHCII(+) microglia and macrophages and formation of microglial nodules. Low or moderate density perivascular cuffs of mononuclear leukocytes were also noted in sa-WM Close and sa-WM Far regions. We did not observe tissue infiltration by T-lymphocytes in the studied ROIs except in T2T1MTR chronic lesions.

It is important to note that sa-WM is different both radiologically and pathologically from "dirty appearing white matter" (DAWM).(17;38) Radiologically, DAWM is defined as WM with diffusely abnormal signal intensity on T2-weighted weighted images, whereas sa-WM has normal T2 signal intensity. Like sa-WM regions, DAWM is located outside of focally demyelinated plaques and has lower MTR than NAWM.(17) However, unlike sa-WM, DAWM is associated with prominent loss of myelin, chronic fibrillary gliosis, presence of inflammatory infiltrates and blood-brain barrier alterations.(38-40) Therefore, it is expected that there would be differences in the pathologic characteristics that determine MRI abnormalities in sa-WM and DAWM, and the findings in these two distinct types of non-lesional MS brain tissue cannot be directly compared.

In this study, subtypes of NAWM regions were defined based on MTR and distance to lesions. Demyelination has been proposed to be the major pathologic substrate for decreased MTR within MS lesions,(29) and our findings of relatively strong correlations between MTR and myelin density across all ROIs are consistent with previous reports. However, additional pathologic features may contribute to the MTR signal.(27)(32;34) When we excluded lesions from the analysis, MTR was no longer correlated with myelin density, suggesting that other pathologic processes were responsible for MTR differences in

NAWM. In non-lesional WM where myelin is preserved, we mainly observed differences in axonal pathology and activated microglia in regions with slightly abnormal MTR as compared to NAWM with normal MTR. To our knowledge, there have not been prior studies on the pathologic correlates of abnormal MRI measures in NAWM as there have been for lesions.

We also investigated pathologic correlates of DTI measurements because DTI is another method used to quantify tissue damage in NAWM in vivo. Pathologic correlates of DTI changes have also been described in lesions, (42;43)(44) but not in non-lesional WM of MS brains. The current study used *in situ* imaging, short post-mortem intervals, and contrast ratios to minimize the potential impact of post-mortem changes in DTI measures.(45-47) In our analysis of DTI parameters across all ROIs (non-lesional WM and focally demyelinated lesions), FA, MD, $\lambda\parallel$ and $\lambda\perp$ were all moderately correlated with markers of myelin and axonal damage, but not with enlarged microglia/macrophages. Interestingly, in the non-lesional regions, decreases in FA and $\lambda\parallel$ were associated with activated microglia and the presence of microglial nodules. There was also a trend for a correlation between MD and axonal count in the non-lesional regions. Overall, these results suggest that in non-lesional WM, subtle increases in MD may be indicative of axonal loss, and decreases in FA and $\lambda\parallel$ may signal microglial activation.

Importantly, we also found that many sa-WM far ROIs were located near cortical lesions. These ROIs were associated with microglial activation. We also noted variable numbers of dystrophic swollen axons in sa-WM far ROIs without significant differences as compared with NAWM. Previous MRI and histopathologic studies suggested that grey matter and white matter abnormalities might occur largely independently from each other, or evolve in different time frames.(3;48;49) It is plausible, however, that activated microglia and secondary axonal degeneration in sa-WM Far regions might be causally related to nearby cortical pathology.

In summary, this study addresses a previously unexplored question: What are the pathologic substrates of subtle MRI changes consistently observed in MS NAWM *in vivo*, including the slight downward shift in the MTR histogram and changes in DTI measurements? Due to the strong correlations between MTR and myelin in lesions, shifts in the MTR histogram are often assumed to be due to changes in myelin. However, in non-lesional WM we did not observe differences in MBP immunoreactivity between NAWM regions with different MTRs. Our data suggest that subtle MTR abnormality in NAWM in close proximity to WM lesions can be attributed to axonal degeneration and microglial activation. In contrast, subtle MTR abnormalities in NAWM far from lesions are associated with marked microglial activation but not with axonal pathology. Previous studies show that MTR and DTI abnormalities in MS NAWM correlate with disability, but are not altered by currently available treatments.(6;7) A better understanding of the substrate for these changes may lead to more targeted imaging outcome measures for new therapies that target secondary axonal damage and microglial activation in NAWM.

Supplementary Material

Refer to Web version on PubMed Central for supplementary material.

Acknowledgments

This study was supported by the National Institute of Health, National Institute of Neurological Disorders and Stroke, P50 NS 38667 (R.M.R., PI; EF Project 3 Leader).

References

(1). Noseworthy JH, Lucchinetti C, Rodriguez M, Weinshenker BG. Multiple sclerosis. New England Journal of Medicine. Sep 28; 2000 343(13):938–52. [Review] [104 refs]. [PubMed: 11006371]

(2). Kutzelnigg A, Lassmann H. Cortical lesions and brain atrophy in MS. Journal of the Neurological Sciences. Jun 15; 2005 233(1-2):55–9. [Review] [62 refs]. [PubMed: 15893328]

(3). Kutzelnigg A, Lucchinetti CF, Stadelmann C, Bruck W, Rauschka H, Bergmann M, et al. Cortical demyelination and diffuse white matter injury in multiple sclerosis. Brain. Nov; 2005 128(Pt 11): 2705–12. [PubMed: 16230320]

(4). Frohman EM, Racke MK, Raine CS. Multiple sclerosis--the plaque and its pathogenesis. New England Journal of Medicine. Mar 2; 2006 354(9):942–55. [Review] [74 refs]. [PubMed: 16510748]

(5). Ludwin SK. The pathogenesis of multiple sclerosis: relating human pathology to experimental studies. Journal of Neuropathology & Experimental Neurology. Apr; 2006 65(4):305–18. [Review] [76 refs]. [PubMed: 16691112]

(6). Richert ND, Ostuni JL, Bash CN, Duyn JH, McFarland HF, Frank JA. Serial whole-brain magnetization transfer imaging in patients with relapsing-remitting multiple sclerosis at baseline and during treatment with interferon beta-1b. Ajnr: American Journal of Neuroradiology. 1998; (9):1705–13. [PubMed: 9802494]

(7). Inglese M, van Waesberghe JH, Rovaris M, Beckmann K, Barkhof F, Hahn D, et al. The effect of interferon beta-1b on quantities derived from MT MRI in secondary progressive MS. Neurology. Mar 11; 2003 60(5):853–60. [PubMed: 12629246]

(8). Allen IV, McQuaid S, Mirakhur M, Nevin G. Pathological abnormalities in the normal-appearing white matter in multiple sclerosis. Neurological Sciences. Apr; 2001 22(2):141–4. [Review] [25 refs]. [PubMed: 11603615]

(9). Evangelou N, Konz D, Esiri MM, Smith S, Palace J, Matthews PM. Regional axonal loss in the corpus callosum correlates with cerebral white matter lesion volume and distribution in multiple sclerosis. Brain. Sep; 2000 123(Pt 9):1845–9. [PubMed: 10960048]

(10). Evangelou N, Konz D, Esiri MM, Smith S, Palace J, Matthews PM. Size-selective neuronal changes in the anterior optic pathways suggest a differential susceptibility to injury in multiple sclerosis. Brain. Sep; 2001 124(Pt 9):1813–20. [PubMed: 11522583]

(11). Filippi M, Paty DW, Kappos L, Barkhof F, Compston DA, Thompson AJ, Zhao GJ, Wiles CM, McDonald WI, Miller DH. Correlations between changes in disability and T2-weighted brain MRI activity in multiple sclerosis: a follow-up study. Neurology. 1995; 45(2):255–60. [PubMed: 7854522]

(12). Rovaris M, Bozzali M, Santuccio G, Ghezzi A, Caputo D, Montanari E, et al. In vivo assessment of the brain and cervical cord pathology of patients with primary progressive multiple sclerosis. Brain. Dec; 2001 124(Pt 12):2540–9. [PubMed: 11701606]

(13). McFarland HF, Barkhof F, Antel J, Miller DH. The role of MRI as a surrogate outcome measure in multiple sclerosis. Multiple Sclerosis. 2002; 8(1):40–51. [PubMed: 11936488]

(14). Bar-Zohar D, Agosta F, Goldstaub D, Filippi M. Magnetic resonance imaging metrics and their correlation with clinical outcomes in multiple sclerosis: a review of the literature and future perspectives. Multiple Sclerosis. Jul; 2008 14(6):719–27. [Review] [116 refs]. [PubMed: 18424478]

(15). Miller DH, Thompson AJ, Filippi M. Magnetic resonance studies of abnormalities in the normal appearing white matter and grey matter in multiple sclerosis. Journal of Neurology. Dec; 2003 250(12):1407–19. [Review] [125 refs]. [PubMed: 14673572]

(16). Ciccarelli O, Werring DJ, Barker GJ, Griffin CM, Wheeler-Kingshott CA, Miller DH, et al. A study of the mechanisms of normal-appearing white matter damage in multiple sclerosis using diffusion tensor imaging--evidence of Wallerian degeneration. J Neurol. Mar; 2003 250(3):287–92. [PubMed: 12638018]

(17). Ge Y, Grossman RI, Babb JS, He J, Mannon LJ. Dirty-appearing white matter in multiple sclerosis: volumetric MR imaging and magnetization transfer ratio histogram analysis. Ajnr: American Journal of Neuroradiology. Nov;-Dec; 2003 24(10):1935–40. [PubMed: 14625213]

(18). Filippi M, Campi A, Dousset V, Baratti C, Martinelli V, Canal N, et al. A magnetization transfer imaging study of normal-appearing white matter in multiple sclerosis. Neurology. Mar; 1995 45(3 Pt 1):478–82. [PubMed: 7898700]

(19). Davie CA, Barker GJ, Thompson AJ, Tofts PS, McDonald WI, Miller DH. 1H magnetic resonance spectroscopy of chronic cerebral white matter lesions and normal appearing white matter in multiple sclerosis. Journal of Neurology, Neurosurgery & Psychiatry. Dec; 1997 63(6): 736–42.

(20). Droogan AG, Clark CA, Werring DJ, Barker GJ, McDonald WI, Miller DH. Comparison of multiple sclerosis clinical subgroups using navigated spin echo diffusion-weighted imaging. Magnetic Resonance Imaging. Jun; 1999 17(5):653–61. [PubMed: 10372518]

(21). Stevenson VL, Parker GJ, Barker GJ, Birnie K, Tofts PS, Miller DH, et al. Variations in T1 and T2 relaxation times of normal appearing white matter and lesions in multiple sclerosis. Journal of the Neurological Sciences. Sep 15; 2000 178(2):81–7. [PubMed: 11018698]

(22). Leary SM, Silver NC, Stevenson VL, Barker GJ, Miller DH, Thompson AJ. Magnetisation transfer of normal appearing white matter in primary progressive multiple sclerosis. Multiple Sclerosis. Oct; 1999 5(5):313–6. [PubMed: 10516773]

(23). van Buchem MA, McGowan JC, Kolson DL, Polansky M, Grossman RI. Quantitative volumetric magnetization transfer analysis in multiple sclerosis: estimation of macroscopic and microscopic disease burden. Magnetic Resonance in Medicine. Oct; 1996 36(4):632–6. [PubMed: 8892218]

(24). Traboulsee A, Dehmeshki J, Peters KR, Griffin CM, Brex PA, Silver N, et al. Disability in multiple sclerosis is related to normal appearing brain tissue MTR histogram abnormalities. Multiple Sclerosis. Dec; 2003 9(6):566–73. [PubMed: 14664468]

(25). Agosta F, Rovaris M, Pagani E, Sormani MP, Comi G, Filippi M. Magnetization transfer MRI metrics predict the accumulation of disability 8 years later in patients with multiple sclerosis. Brain. Oct; 2006 129(Pt 10):2620–7. [PubMed: 16951409]

(26). Dousset V, Brochet B, Vital A, Gross C, Benazzouz A, Boullerne A, et al. Lysolecithin-induced demyelination in primates: preliminary in vivo study with MR and magnetization transfer. Ajnr: American Journal of Neuroradiology. Feb; 1995 16(2):225–31. [PubMed: 7726066]

(27). Brochet B, Dousset V. Pathological correlates of magnetization transfer imaging abnormalities in animal models and humans with multiple sclerosis. Neurology. 1999; 53(5 Suppl 3):S12–7. [Review] [17 refs]. [PubMed: 10496205]

(28). Barkhof F, Bruck W, De Groot CJ, Bergers E, Hulshof S, Geurts J, Polman CH, van der Valk P. Remyelinated lesions in multiple sclerosis: magnetic resonance image appearance. Archives of Neurology. 2003; 60(8):1073–81. [PubMed: 12925362]

(29). Schmierer K, Scaravilli F, Altmann DR, Barker GJ, Miller DH. Magnetization transfer ratio and myelin in postmortem multiple sclerosis brain. Annals of Neurology. Sep; 2004 56(3):407–15. [PubMed: 15349868]

(30). Filippi M, Rocca MA, Martino G, Horsfield MA, Comi G. Magnetization transfer changes in the normal appearing white matter precede the appearance of enhancing lesions in patients with multiple sclerosis. Ann Neurol. Jun; 1998 43(6):809–14. [PubMed: 9629851]

(31). Vrenken H, Geurts JJ, Knol DL, Polman CH, Castelijns JA, Pouwels PJ, et al. Normal-appearing white matter changes vary with distance to lesions in multiple sclerosis. Ajnr: American Journal of Neuroradiology. Oct; 2006 27(9):2005–11. [PubMed: 17032884]

(32). Fisher E, Chang A, Fox RJ, Tkach JA, Svarovsky T, Nakamura K, et al. Imaging correlates of axonal swelling in chronic multiple sclerosis brains. Annals of Neurology. Sep; 2007 62(3):219–28. [PubMed: 17427920]

(33). Moll NM, Cossoy MB, Fisher E, Staugaitis SM, Tucky BH, Rietsch AM, et al. Imaging correlates of leukocyte accumulation and CXCR4/CXCL12 in multiple sclerosis. Archives of Neurology. Jan; 2009 66(1):44–53. [PubMed: 19139298]

(34). Young EA, Fowler CD, Kidd GJ, Chang A, Rudick R, Fisher E, et al. Imaging correlates of decreased axonal Na+/K+ ATPase in chronic multiple sclerosis lesions. Annals of Neurology. Apr; 2008 63(4):428–35. [PubMed: 18438950]

(35). Fisher E, Cothren RM, Tkach JA, Masaryk TJ, Cornhill JF. Knowledge-based 3D segmentation of MR images for quantitative MS lesion tracking. SPIE Medical Imaging. 1997; 3034:19–25.

(36). Trapp BD, Peterson J, Ransohoff RM, Rudick R, Mork S, Bo L. Axonal transection in the lesions of multiple sclerosis. New England Journal of Medicine. 1998; 338(5):278–85. [PubMed: 9445407]

(37). Lovas G, Szilagyi N, Majtenyi K, Palkovits M, Komoly S. Axonal changes in chronic demyelinated cervical spinal cord plaques. Brain. Feb; 2000 123(Pt 2):308–17. [PubMed: 10648438]

(38). Seewann A, Vrenken H, van d V, Blezer EL, Knol DL, Castelijns JA, et al. Diffusely abnormal white matter in chronic multiple sclerosis: imaging and histopathologic analysis. Archives of Neurology. May; 2009 66(5):601–9. [PubMed: 19433660]

(39). Moore, GR Wayne. MRI-clinical correlations: more than inflammation alone-what can MRI contribute to improve the understanding of pathological processes in MS? Journal of the Neurological Sciences. 2003; 206(2):175–9. [PubMed: 12559507]

(40). Vos CM, Geurts JJ, Montagne L, van Haastert ES, Bo L, van d V, et al. Blood-brain barrier alterations in both focal and diffuse abnormalities on postmortem MRI in multiple sclerosis. Neurobiology of Disease. 1920; (3):953–60.

(41). Basser PJ, Pierpaoli C. Microstructural and physiological features of tissues elucidated by quantitative-diffusion-tensor MRI. Journal of Magnetic Resonance Series B. Jun; 1996 111(3): 209–19. [PubMed: 8661285]

(42). Song SK, Yoshino J, Le TQ, Lin SJ, Sun SW, Cross AH, et al. Demyelination increases radial diffusivity in corpus callosum of mouse brain. Neuroimage. May 15; 2005 26(1):132–40. [PubMed: 15862213]

(43). Song SK, Sun SW, Ju WK, Lin SJ, Cross AH, Neufeld AH. Diffusion tensor imaging detects and differentiates axon and myelin degeneration in mouse optic nerve after retinal ischemia. Neuroimage. 2003; (3):1714–22. [PubMed: 14642481]

(44). Budde MD, Kim JH, Liang HF, Schmidt RE, Russell JH, Cross AH, et al. Toward accurate diagnosis of white matter pathology using diffusion tensor imaging. Magnetic Resonance in Medicine. Apr; 2007 57(4):688–95. [PubMed: 17390365]

(45). Sun SW, Liang HF, Le TQ, Armstrong RC, Cross AH, Song SK. Differential sensitivity of in vivo and ex vivo diffusion tensor imaging to evolving optic nerve injury in mice with retinal ischemia. Neuroimage. Sep; 2006 32(3):1195–204. [PubMed: 16797189]

(46). Schmierer K, Wheeler-Kingshott CA, Boulby PA, Scaravilli F, Altmann DR, Barker GJ, et al. Diffusion tensor imaging of post mortem multiple sclerosis brain. Neuroimage. Apr 1; 2007 35(2):467–77. [PubMed: 17258908]

(47). Schmierer K, Wheeler-Kingshott CA, Tozer DJ, Boulby PA, Parkes HG, Yousry TA, et al. Quantitative magnetic resonance of postmortem multiple sclerosis brain before and after fixation. Magnetic Resonance in Medicine. Feb; 2008 59(2):268–77. [PubMed: 18228601]

(48). Bo L, Geurts JJ, van d V, Polman C, Barkhof F. Lack of correlation between cortical demyelination and white matter pathologic changes in multiple sclerosis. Archives of Neurology. Jan; 2007 64(1):76–80. [PubMed: 17210812]

(49). De Stefano N, Matthews PM, Filippi M, Agosta F, De Luca M, Bartolozzi ML, et al. Evidence of early cortical atrophy in MS: relevance to white matter changes and disability. Neurology. Apr 8; 2003 60(7):1157–62. [PubMed: 12682324]

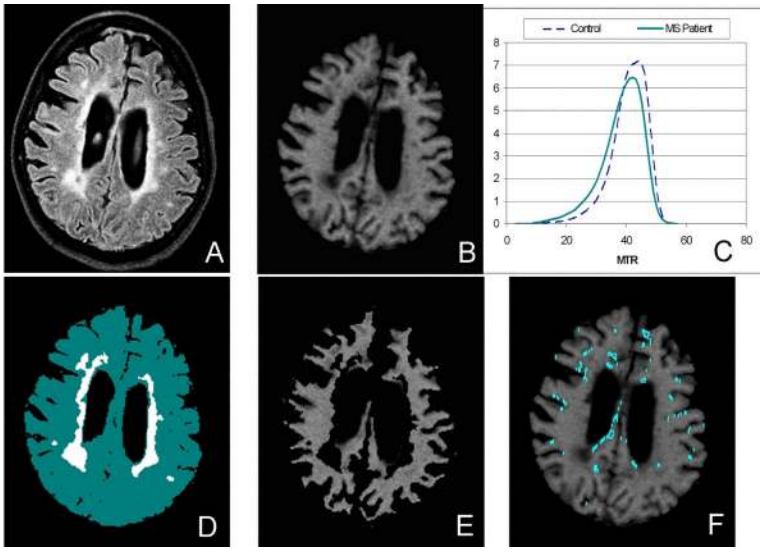

Figure 1.

Example images from an MS tissue donor to demonstrate method used to identify sa-WM ROIs. The FLAIR image (A) and corresponding MTR image (B) are shown, along with typical MTR histograms (C) showing the slight shift to the left for the MS patient as compared to an age-matched control. After the FLAIR image is segmented into normal-appearing white matter and T2-hyperintense lesions (D), the corresponding MTR image (B) is masked (E) and the remaining voxels that fall within the normal-appearing white matter and have MTR values in the range of 90-95% of the mean for NAWM are identified as candidate sa-WM ROIs (F). sa-WM Close and Far ROIs were selected manually from these candidate regions to insure partial volume gray matter voxels were not included.

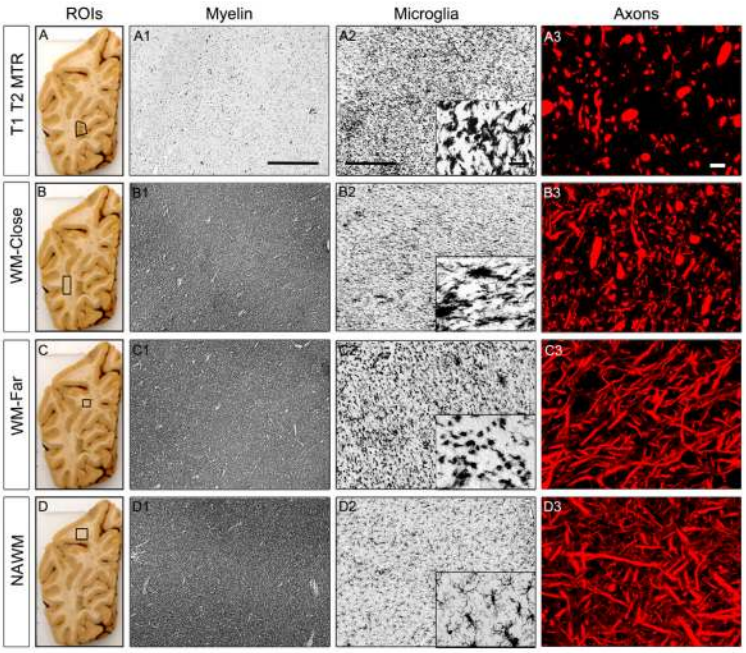

Figure 2.

Histopathological changes in MS regions of interest (ROIs): T2 T1 MTR (A-A3), sa-WM Close (B-B3), sa-WM Far (C-C3) and NAWM (D-D3). Macrographs of MS brain slices with superimposed outlines of studied ROIs are shown in the left panel. Myelin immunoreactivity is reduced in T2 T1 MTR ROIs (A1). Myelin status remains unaltered in sa-WM Close (B1), sa-WM Far (C1) ROIs. The density of activated microglia is increased in T2 T1 MTR ROIs (A2), sa-WM Close (B2), sa-WM Far (C2) as compared with NAWM (D2). Remarkably altered microglial morphology is noted in sa-WM Far as shown on the high-magnification insert, where $MHCII^{+}$ microglia exhibit typical morphology of phagocytic cells. Significant axonal loss and many dystrophic axons are revealed in T2 T1 MTR lesions (A3). Dystrophic and transected axons are also found in sa-WM Close (B3), whilst axonal number and morphology are not significantly modified in sa-WM Far (C3) and NAWM (D3).

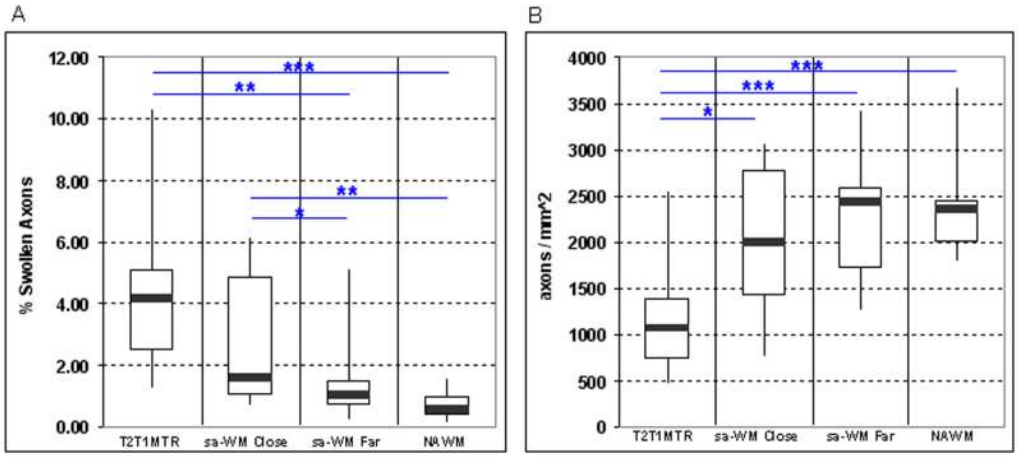

Figure 3.

Pathologically enlarged axons were observed in all 4 types of ROIs. **(A)** The mean percent area occupied by pathologically enlarged axons was highest in T2T1MTR lesions, followed by sa-WM Close, sa-WM Far, and NAWM ROIs. (*p<0.05, **p<0.01, ***p<0.001) **(B)** Numbers of axons were lower in T2T1MTR lesions as compared to sa-WM Close, sa-WM Far and NAWM ROIs. There was a trend (p=0.10) for lower axon counts in sa-WM Close ROIs. (*p<0.05, **p<0.01, ***p<0.001)

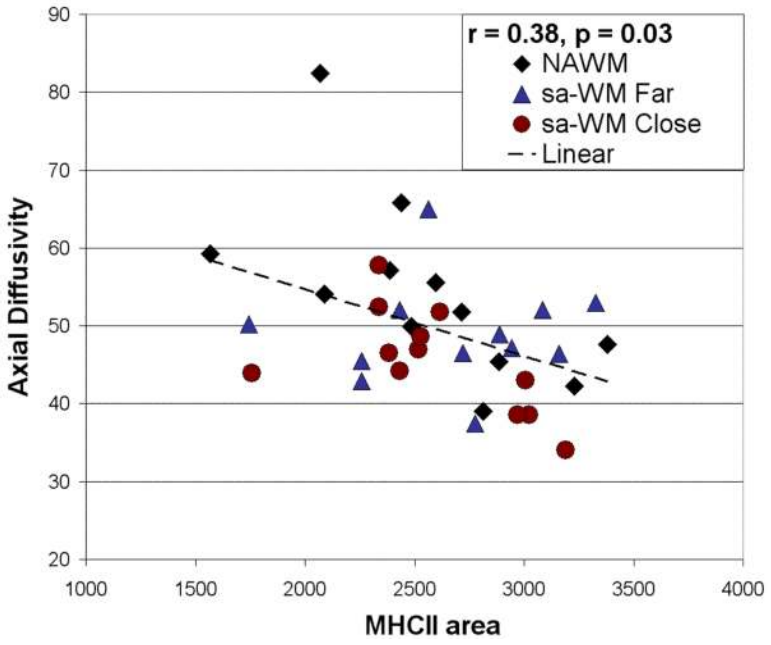

Figure 4.
MHCII(+) cell areas and axial diffusivity, demonstrating correlations in sa-WM and NAWM ROIs.

Table 1

Primary antibodies used for immunohistochemical analysis.

Antibody	Cat#	Clone	Isotype	Host	Dilution	Company
MBP	SMI-94	SMI-91	IgG1	mouse	1:100	Covance, Emeryville, CA, USA
MHCII	M0775	CR3/43	IgG1κ	mouse	1:100	DakoCytomation, Golstrup, Denmark
GFAP	Z0334	-/-	IgG	rabbit	1:2000	DakoCytomation, Golstrup, Denmark
Neurofilaments-H	AHP246	-/-	IgG	rabbit	1:500	Serotec, Raleigh, NC, USA
Glut-1	AB1340	-/-	IgG	rabbit	1:500	Millipore, Billerica, MA, USA
IgG	BA-3000	-/-	IgG	goat	1:100	Vector Laboratories, CA, USA

Table 2

Clinical data on MS patients in studied MS material.

Brain#	Age (years)	Gender	Disease Duration (years)	EDSS at time of death	Brain Weight (g)	Post-mortem time (h)
MS37	65	M	46	8.5	1300	4.5
MS41	41	F	14	8.0	1300	5.5
MS42	52	F	19	6.5	1120	6
MS44	52	M	30	9.0	1150	7
Summary / Mean±SD	**52.5±9.8**	**2 male 2 female**	**27.2±14.2**	**8±1.1**	**1217.5±96.0**	**5.8±1.0**

*EDSS – Expanded Disability Status Score.

Table 3

Spearman Partial Correlations between MRI and Pathologic Characteristics (with significant correlations in **bold** type)

All ROIs (n=48)	MTR	MD	FA	Axial Diffusivity	Radial Diffusivity
Myelin density	**0.63 (p<0.0001)**	**−0.58 (p<0.0001)**	**0.38 (p=0.008)**	**−0.41 (p=0.004)**	**−0.52 (p=0.0002)**
Axonal density	**0.58 (p<0.0001)**	**−0.53 (p=0.0002)**	**0.42 (p=0.003)**	**−0.50 (p=0.0003)**	**−0.59 (p<0.0001)**
Axonal area	**−0.46 (p=0.001)**	**0.47 (p=0.0008)**	**−0.41 (p=0.004)**	**0.38 (p=0.008)**	**0.46 (p=0.001)**
MHC II (+) area	−0.14 (p=0.35)	−0.072 (p=0.63)	−0.17 (p=0.26)	−0.14 (p=0.33)	0.16 (p=0.30)
NAWM and sa ROIs only (n=36)	**MTR**	**MD**	**FA**	**Axial Diffusivity**	**Radial Diffusivity**
Myelin density	0.16 (p=0.37)	−0.19 (p=0.28)	0.14 (p=0.42)	−0.08 (p=0.66)	−0.25 (p=0.15)
Axonal density	0.22 (p=0.21)	−0.32 (p=0.06)	0.20 (p=0.24)	−0.25 (p=0.15)	−0.27 (p=0.11)
Axonal area	0.06 (p=0.73)	0.14 (p=0.43)	−0.23 (p=0.18)	−0.011 (p=0.95)	0.08 (p=0.65)
MHC II (+) area	−0.19 (p=0.26)	−0.16 (p=0.36)	**−0.33 (p=0.05)**	**−0.38 (p=0.03)**	0.12 (p=0.50)

* ROI = regions of interest; MTR = magnetization transfer ratio; MD = mean diffusivity; FA = fractional anisotropy

Table 4

Number of activated MHCII(+) cells in MS ROIs.

Imaging characteristics	T2T1MTR	sa-WM Close	sa-WM Far	NAWM
Total number of MHCII cell	3866	4298	4621	3979
MHCII cell area >5000px^2	831 (21%)***	765 (17.8%)***	791 (17%)***	596 (15%)

*** p<0.001 in T2T1MTR, sa-WM Close, sa-WM Far as compared with NAWM